DC Bus Voltage Regulation Using Photovoltaic Module: A Non-Iterative Method

Alireza Askarian[1,a], Mayank Baranwal[1,b] and Srinivasa Salapaka[1,c]

Abstract— **Uncertainties in load power demand and unpredictabilities associated with renewable energy sources pose challenges to current microgrids. The situation worsens when the maximum power generated by a Photovoltaic (PV) module exceeds the power demanded by the load. The excess power increases the voltage at the point of common coupling (PCC). This paper addresses the issue of DC-link voltage regulation using a standalone PV module for the scenario when PV output at maximum power point (MPP) exceeds load demands. In particular, the time-scale separation between the fast PV dynamics and the slow variations in weather (temperature and irradiance) conditions is exploited to devise a novel non-iterative control strategy with fast closed-loop dynamics. A disturbance-rejection based robust control framework is employed and the closed-loop voltage regulation and load disturbance rejection performances are compared for the constant current and the constant voltage modes of operation of a PV module. Simulation case studies are presented which examine effectiveness and robustness of controllers for voltage regulation at the PCC.**

I. INTRODUCTION

Microgrids comprise of localized group of loads and power sources such as PV, battery, wind turbine and provide local power to local loads while increasing power efficiency by reducing losses in transmission lines. Fig. 1 represents a simplified schematic of microgrid system. In such a microgrid, several power sources are connected to PCC via paralleled DC/DC converters. Such a parallelization not only provides more power from different sources for large loads, it also gives the system more robustness in case of failure of one of the converters. The DC-link can be interfaced further through a DC/AC inverter to an AC-link which provides power to AC loads or injects power into the utility grid when operated in grid-tied mode.

Most of the loads are rated for some nominal operating voltage. Any deviation from nominal voltage can cause malfunction or damage to the load. Hence one of the main goals in microgrids is the regulation of DC-link voltage to predefined setpoint with robustness to disturbances present in such systems. Voltage regulation in microgrids can be studied in two cases - (a) $\text{Power}_{\text{PV}} < \text{Power}_{\text{load}}$ and (b) $\text{Power}_{\text{PV}} > \text{Power}_{\text{load}}$.

In the first case, power consumption at the PCC is more than the maximum power point (MPP) of the PV module, therefore other power sources such as battery provide additional power required by the load. In this case, voltage regulation at the DC-link is typically achieved through a coordinated control of DC/DC converters [1] connected to power storage devices. However, DC/DC converter interfacing PV to the DC-link is configured for maximum power point tracking (MPPT) to maximize power provided by PV module. The output *I-V* (current-voltage) characteristics of a PV module as shown in Fig. 3a is nonlinear. In order to track the maximum power point, MPPT algorithms such as perturb and observe (P&O) [2] or more sophisticated incremental conductance (IC) [3] are used. These MPPT methods are based on iterative function maximization techniques such as hill climbing algorithm [4]. However, the iterative algorithms introduce oscillations around MPP at the steady state and have relatively longer tracking time. Therefore these methods are only designed to maximize fraction of power provided by PV; they cannot be employed for critical operations such as regulation of output voltage at the DC-link.

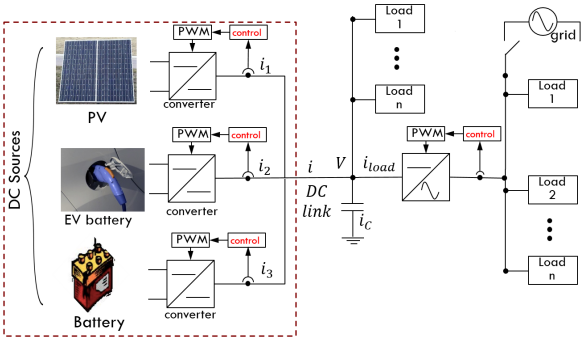

Fig. 1: Simple schematic of a microgrid. Set of localized DC power sources provide power at common DC-link.

In the second case, which is the primary topic of this paper, power generation of PV at MPP is greater than power required by load. Therefore, if a PV interfaced DC/DC converter is controlled by any MPPT algorithm, power imbalance between source (PV) and load will result in an increase in voltage at the DC-link. This excess power forces voltage regulating DC/DC converters to reduce their current injections to zero; hence losing their voltage regulating capability. This problem can be avoided by having power storage that

[1]Department of Mechanical Science and Engineering, University of Illinois at Urbana-Champaign, 61801 IL, USA
{[a]askaria2, [b]baranwa2, [c]salapaka}@illinois.edu
Supported by: ARPAE-E NODES Program

can take in excess power to compensate for the power imbalance; however this option can add significant costs. In this paper, we address the objective of voltage regulation at the DC-link using only a standalone PV module.

This is achieved by restricting the PV module to operate in certain prespecified regions on the *I-V* curves and describing dynamical models for the DC/DC interfaced PV in each of these regions. The algebraic structure facilitates synthesis of model-based controllers by exploiting the time-scale separation between the fast PV dynamics and the slow temporal variations in weather conditions. Another significant aspect of the proposed work is the adoption of disturbance-rejection framework for synthesizing model-based controllers. This framework allows for regulation of the DC-link voltage without requiring the output loading conditions to be known to the controller.

II. DYNAMICAL MODELING OF PV MODULE

To utilize the algebraic structure of PV output *I-V* characteristics, useful equivalent circuit model of PV module is discussed. Ideal solar panel can be modeled as a current source in parallel with a diode. The *photo-generated current* i_{PV} is modeled as the current source which correlates positively to level of solar irradiance incident on the PV module. However, PV is not ideal and exhibits resistance against current flow and leakage of current through the cell. These effects are captured in the model by including series and parallel resistances R_s and R_p, respectively. Fig. 2 shows a schematic of PV circuit model. Using Kirchhoff's circuit laws, PV output current and voltage are related by

$$i = i_{\text{PV}}(G) - i_D - \frac{v + iR_s}{R_p} \tag{1}$$

$$i_D = i_0 \left\{ \exp\left(\frac{q(v + iR_s)}{nkT} \right) \right\} \tag{2}$$

where i, i_{PV}, i_0 and i_D are output current, photo-generated current which is function of solar irradiance G, diode reverse saturation current, and diode current given by the Shockley diode equation (2). The quantities v, q, k, n and T denote the PV output voltage, elementary charge, diode ideality factor, Boltzmann constant and absolute temperature of PV [5]. Photo-generated current i_{PV} and diode current i_D are functions of solar irradiance and ambient temperature, making *I-V* equation time-varying. It is generally difficult to analyze a nonlinear, time-varying system; however in the following subsections, *I-V* equation is analyzed by providing a piecewise linear approximation of *I-V* curve and by exploiting the time-scale separation between the fast PV dynamics and the slow variations in ambient irradiance and temperature.

A. Linearizing PV Model

I-V equation of a PV module described in (1) and (2) can be put into an implicit functional form as

$$f(i, v, T, G) = 0.$$

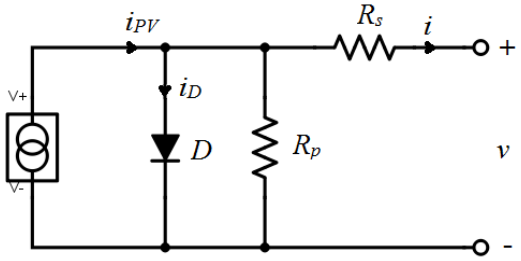

Fig. 2: Ideal PV can be modeled as current source in parallel with diode.

Function f is linearized about an operating point (i_0, v_0, T_0, G_0) by considering first-order Taylor series expansion [6]

$$\alpha_i \tilde{i} + \alpha_v \tilde{v} + \alpha_T \tilde{T} + \alpha_G \tilde{G} = 0, \tag{3}$$

$$i = \left(i_0 - \frac{\alpha_T}{\alpha_i}\tilde{T} - \frac{\alpha_G}{\alpha_i}\tilde{G} \right) - \frac{\alpha_v}{\alpha_i}\tilde{v}, \tag{4}$$

where $\alpha_i, \alpha_v, \alpha_T$, and α_G are first-order Taylor series coefficients evaluated at point (i_0, v_0, T_0, G_0). The quantities $\tilde{i}, \tilde{v}, \tilde{T}$ and $\tilde{G}$ denote the first-order perturbations around the operating point (i_0, v_0, T_0, G_0).

Furthermore, if the PV model is linearized at points $(i_0 = I_{\text{SC}}, v_0 = 0, T_0, G_0)$ and $(i_0 = 0, v_0 = V_{\text{OC}}, T_0, G_0)$, where I_{SC} and V_{OC} denote PV short circuit current and open circuit voltage, respectively (see Fig. 3), then the two resulting linearized models divide *I-V* curve into three regions shown on 3. The first region includes points on *I-V* curve that are well approximated by the linearized model at point $(i_0 = I_{\text{SC}}, v_0 = 0, T_0, G_0)$. This region is referred to as *current source region*; since linearized model at this point behaves as a constant current source with large parallel resistor [7].

$$i = I_{\text{SC}} - \left(\frac{\alpha_T}{\alpha_i}\tilde{T} + \frac{\alpha_G}{\alpha_i}\tilde{G} \right) - \frac{\alpha_v}{\alpha_i} v \tag{5}$$

The second region consist of points that are well approximated by the linearized model at $(i_0 = 0, v_0 = V_{\text{OC}}, T_0, G_0)$. It is not difficult to show that the value of $\frac{\alpha_i}{\alpha_v}$ is small [7], and hence (4) can be rewritten as

$$v = V_{\text{OC}} - \left(\frac{\alpha_T}{\alpha_v}\tilde{T} + \frac{\alpha_G}{\alpha_v}\tilde{G} \right) - \frac{\alpha_i}{\alpha_v} i, \tag{6}$$

which is an equivalent circuit model for constant voltage source with small series resistor. Hence, this region is referred to as *voltage source region* of *I-V* curve. The third region, which comprises of MPP and the neighboring region, is highly nonlinear and thus cannot be approximated by either of the two aforementioned linearized models. Since this paper addresses the scenario when the PV output at MPP exceeds the power required by the load at the DC-link, the PV point of operation in this work deviates from MPP; hence the linearized models are utilized to describe the dynamics of a PV module and synthesize controllers for voltage regulation at the DC-link.

B. I-V and P-V Characteristics of PV

I-V characteristic of a PV module is both nonlinear and time varying. Change in level of solar irradiance dramatically changes photo-generated current. This change is usually caused by movements of the sun and clouds. Fig. 3 shows *I-V* and *P-V* (power-voltage) curves of a PV module for different irradiance levels.

In the current source region and under stable weather conditions, (5) holds. However, value of I_{SC} is a function of irradiance and increases with increase in solar irradiance. Similarly in the voltage source region, the linearized model given by (6) holds. V_{OC} is also function of irradiance.

Although, variations in system parameters due to changes in weather conditions presents difficulty, it is overcome by exploiting time-scale separation between the fast PV dynamics and the slow weather dynamics.

Note that solar irradiance has comparatively faster dynamics than ambient temperature; since solar irradiance is influenced by rapid movement of clouds and the sun. However, if PV controller is designed with sufficiently large bandwidth, temperature and solar irradiance can be approximated by some constant (unknown) parameters, thereby resulting in regulation of the DC-link voltage to the desired setpoint by the PV controller before any significant changes occur in temperature and solar irradiance. With this assumption, PV analysis in this paper is scrutinized by considering constant but *unknown* temperature and solar irradiance.

PV module is usually interfaced to DC link via a buck or a boost converter. Buck and boost converters provide a means to change PV operating point, allowing control of PV module. Since the desired DC-link voltage is larger than the open circuit voltage V_{OC} of PV module, this paper discuss the dynamical modeling of only boost converters in the next section.

III. AVERAGED MODELING OF DC-DC BOOST CONVERTER

One of the ways to control the operating point of a PV module is to interface PV to the DC-link via buck or boost converter. In this paper, we discuss interfacing of PV modules via boost converters, however the same analysis can be generalized for buck converters.

Boost converter [8] is a DC/DC power converter that steps up the input voltage while stepping down the current at its output. Boost converter (see Figure 4) is comprised of a DC-link capacitor, an inductor and a semiconductor switching device. Considering the switching nature of DC/DC boost converters, differential equations in open switch and closed switch modes are averaged over a switching cycle and are described by the following averaged model [8]

$$C\frac{dv(t)}{dt} = d'(t)i_L(t) - i_{\text{load}}(t) \tag{7}$$

$$L\frac{di_L(t)}{dt} = v_g(t) - d'(t)v(t), \tag{8}$$

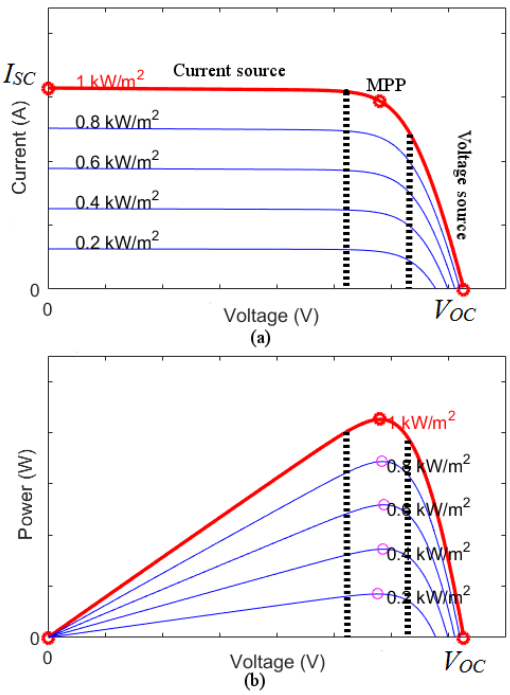

Fig. 3: (a) *I-V* curve can be divided into three regions for different solar irradiance. (b) As shown in the graph, at each solar irradiance level, maximum power is attained at MPP.

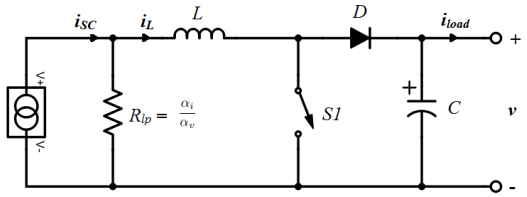

Fig. 4: linearized PV connected to boost converter

where, the quantities $i_L, i_{\text{load}}, v_g$ and v represent averaged (over a switching cycle) values of the inductor current, load current, input voltage and output voltage, respectively. The quantity $d'(t)$ is complimentary duty-cycle defined by $d' = 1 - d$, where d is the duty-cycle of the PWM input applied to switch S_1. Output voltage $v(t)$ is varied by applying PWM signal with variable duty cycle. The following subsection describes averaged dynamical modeling of PV module interfaced with DC/DC boost converter.

A. Boost Converter Interfaced With PV

The dynamical equations of a boost converter interfaced to a PV in the current source region are given by

$$C\frac{dv}{dt} = d'i_L - i_{\text{load}} \tag{9}$$

$$L\frac{di_L}{dt} = (I_{\text{SC}} - i_L)\frac{\alpha_i}{\alpha_v} - d'v \tag{10}$$

The above equations are derived using (5), (7) and (8) by substituting v_g under assumption of constant

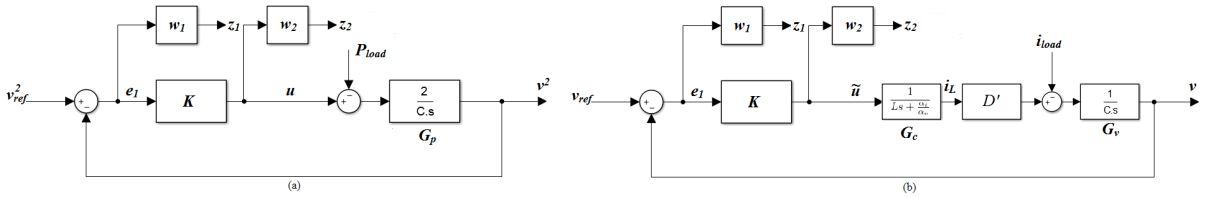

Fig. 5: representation of control design for PV in (a) current source region (b) voltage source region

weather ($\tilde{G}$=$\tilde{T}$=0). A similar analysis of PV in the constant voltage region yields (from (6))

$$C\frac{dv}{dt} = d^{'} i_L - i_{\text{load}} \tag{11}$$

$$L\frac{di_L}{dt} = V_{\text{OC}} - \frac{\alpha_i}{\alpha_v} i_L - d^{'} v. \tag{12}$$

We now proceed to control design and synthesis in the next section.

IV. CONTROLLER DESIGN

Controllers are synthesized using a stacked mixed-sensitivity $\mathcal{H}_\infty$ framework.

A. PV Controller for Voltage source region

The design for PV controller in the voltage source region is inherited from our previous work [1]. By defining $D' = \frac{V_{\text{OC}}}{V_{\text{ref}}}$, where V_{ref} is the desired output voltage and V_{OC} is PV open circuit voltage (same as the input voltage of the boost converter), (11) and (12) can be rewritten as

$$C\frac{dv}{dt} = \underbrace{(D^{'} + \hat{d}^{'}(t))}_{\approx D^{'}} i_L - i_{\text{load}} \tag{13}$$

$$L\frac{di_L}{dt} + \frac{\alpha_i}{\alpha_v} i_L = \underbrace{V_{\text{OC}} - d^{'}(t) v}_{\tilde{u}(t) := V_{\text{OC}} - u(t)}. \tag{14}$$

Here $\hat{d}^{'} = d^{'} - D^{'}$ is considered to be small, allowing for linear approximation around steady-state complementary duty cycle $D^{'}$ given by

$$C\frac{dv}{dt} = D^{'} i_L - i_{\text{load}} \tag{15}$$

$$L\frac{di_L}{dt} + \frac{\alpha_i}{\alpha_v} i_L = \tilde{u}, \tag{16}$$

where $\tilde{u}(t)$ is the control input. For better voltage tracking at the DC-link, a controller must ensure that the voltage regulation error $e_1 = V_{\text{ref}} - v$ is small irrespective of the load disturbance i_{load} and the control effort is not saturated. These objectives are met by posing a multi-objective optimization problem, where the required objectives are formulated in terms of the norms of transfer functions in a stacked framework as described below. From Fig. 5 the matrix transfer function from exogenous inputs $V_{\text{ref}}, i_{\text{load}}$ and control variable $\tilde{u}$ to regulated outputs z_1, z_2, and input to the controller e_1 is given by

$$\begin{bmatrix} z_1 \\ z_2 \\ e_1 \end{bmatrix} = \begin{bmatrix} w_1 & w_1 G_v & -w_1 D^{'} G_v G_c \\ 0 & 0 & w_2 \\ 1 & G_v & -D^{'} G_v G_c \end{bmatrix} \begin{bmatrix} V_{\text{ref}} \\ i_{\text{load}} \\ \tilde{u} \end{bmatrix} \tag{17}$$

The optimization problem is to find stabilizing controller K that minimizes $\mathcal{H}_\infty$-norm of the above matrix transfer function. Weight functions w_1 and w_2 are chosen to reflect design specifications of robustness to parametric uncertainties, tracking bandwidth and saturation limits on the control signal.

B. PV Controller for Current source region

Note that (9) and (10) are coupled nonlinear equations in v and i_L. Multiplying (9) by v and (10) by i_L we obtain

$$\frac{1}{2} C \frac{dv^2}{dt} = \underbrace{d^{'}(t) i_L v}_{u(t)} - \underbrace{i_{\text{load}} v}_{P_{\text{load}}} \tag{18}$$

$$\frac{1}{2} L \frac{di_L^2}{dt} = \left(I_{\text{SC}} i_L - i_L^2 \right) \frac{\alpha_i}{\alpha_v} - \underbrace{d^{'}(t) i_L v}_{u(t)} \tag{19}$$

In (18) and (19) inductor current i_L and output voltage v are measured values and no assumption is made regarding value of i_{load}; hence $v i_{\text{load}}$ is treated as a disturbance (power) signal P_{load}. In addition $u = d^{'} i_L v$ is regarded as the control input. The PWM duty-cycle $d(t)$ can be obtained from $u(t)$ by, $d(t) = 1 - \frac{u(t)}{i_L(t) v(t)}$. It should be remarked that the complementary duty-cycle is given by $d^{'}(t) = D^{'} + \hat{d}^{'}(t)$, where $D^{'}$ is the nominal duty-cycle and satisfies $D' \leq \frac{V_{\text{OC}}}{V_{\text{ref}}} < 1$ for given weather and output load ,and $\hat{d}^{'}(t)$ is very small, thereby ensuring that the duty-cycle $d(t) \in [0, 1]$. Therefore, (18) and (19) can be rewritten as

$$\frac{1}{2} C \frac{dv^2}{dt} = u - P_{load} \tag{20}$$

$$\frac{1}{2} L \frac{di_L^2}{dt} = (I_{SC} i_L - i_L^2) \frac{\alpha_i}{\alpha_v} - u \tag{21}$$

Note that (20) and (21) are in fact power balance equations and capture the change in the energy of capacitor and inductor respectively. Furthermore, both the equations share the same control effort $u(t)$. Since the reference for the inductor current is not known apriori and the output voltage is required to be regulated to V_{ref}, the controllers are synthesized by considering only (20) as a basis for control design. In fact, it suffices to synthesize controller for the capacitor power balance equation (20) since regulating DC-link voltage ensures the averaged value of inductor current converges to some nominal value. Thus ensuring

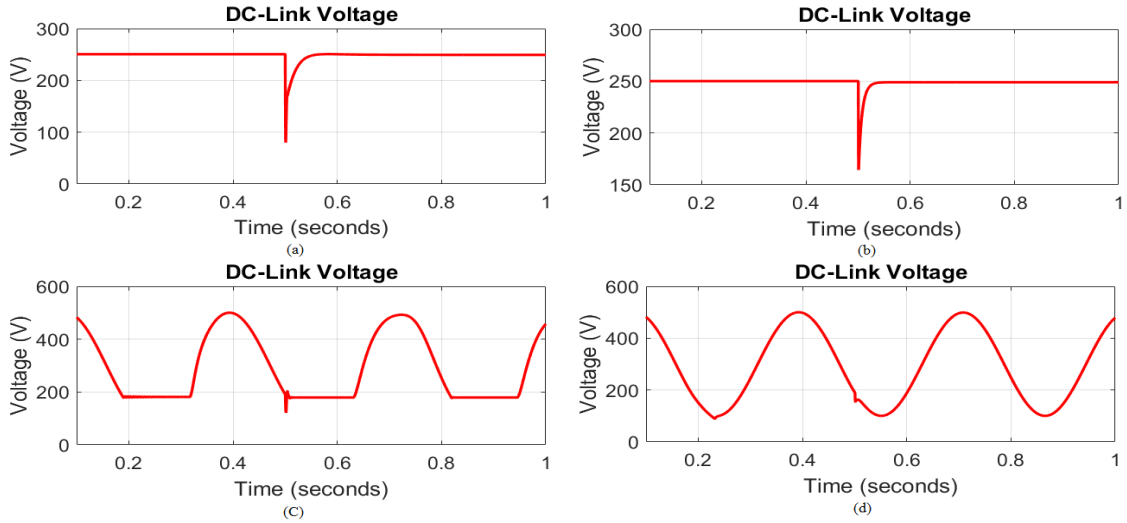

Fig. 6: DC link voltage regulation using standalone PV in (a) voltage source region (b) current source region. DC link voltage set point tracking in (c) voltage source region (d) current source region.

stability of (20) renders the closed-loop system in (21) stable. This observation is formalized in the following claim.

Claim 1: If the DC-link voltage v is regulated to V_{ref}, then the averaged inductor current i_L is bounded and converges to some nominal value I_L locally.
Proof: See Appendix for details. As stated previously, the main objective for the design of controller K (shown in Fig. 5) is to ensure small tracking error e_1, while simultaneously reject disturbance power P_{load}. These objectives are again formulated in terms of the norm of matrix transfer function described below.

$$\begin{bmatrix} z_1 \\ z_2 \\ e_1 \end{bmatrix} = \begin{bmatrix} w_1 & w_1 G_p & -w_1 G_p \\ 0 & 0 & w_2 \\ 1 & G_p & -G_p \end{bmatrix} \begin{bmatrix} v_{ref}^2 \\ P_{\text{load}} \\ u \end{bmatrix} \tag{22}$$

As before, the weight functions w_1 and w_2 are chosen to reflect similar design specifications such as tracking bandwidth and saturation limits on control signal. In the next section, we discuss simulation case studies to validate the effectiveness of the proposed control design in terms of robustness to modeling and parametric uncertainties and fast DC-link voltage regulation in presence of time-varying (unknown to the controller) loads.

V. CASE STUDIES: SIMULATIONS AND DISCUSSIONS

In this section simulation results are reported in order to assess the performance of proposed control design. All simulations are performed using MATLAB/Simulink utilizing SimPower libraries.

The effectiveness of the proposed control design is well illustrated by considering a challenging practical scenario with (*unknown*) step changes in load, large (20%) uncertainties in inductance and capacitance values, and unknown ambient temperature and solar irradiance. Specifically, we consider the following simulation parameters:

Converter Parameters:
- Actual Inductance and Capacitance: $L = 1.2\text{mH}$, $C = 600\mu\text{F}$
- Design Inductance and Capacitance: $L = 1.0\text{mH}$, $C = 500\mu\text{F}$

PV Parameters:
- 80 strings of 5 series 1Soltech1STH-215-P
- Unknown irradiance: 1kW/m^2
- Peak Power: 85.25kW
- V_{OC}: $\sim$ 181V
- Maximum I_{SC}: 627.2A

Other Simulation Parameters:
- Total simulation time: 1s
- Case 1:
  Constant $V_{\text{ref}} = 250\text{V}$
  Load requirements:
  6.5kW, for $t < 0.5\text{s}$, 68.25kW, for $t \geq 0.5\text{s}$
- Case 2:
  Sinusoidal $V_{\text{ref}} = 300 + 200\sin(20t)\text{V}$
  Load:
  100Ω, for $t < 0.5\text{s}$, 3Ω, for $t \geq 0.5\text{s}$

A. Voltage Regulation under Sudden Load Change, Parametric Uncertainties and Varying Irradiance

In the first case, synthesized controllers for both the voltage source and the current source regions are tested for robustness to parametric uncertainty (uncertainties in L and C), voltage regulation performance under load disturbance and irradiance variation. Irradiance is provided as a ramp input with an initial value of 300W/m^2 and a slope of $1000\text{W/m}^2\text{s}$. Figs. 6 (a) and (b) show DC-link voltage regulation in PV voltage source

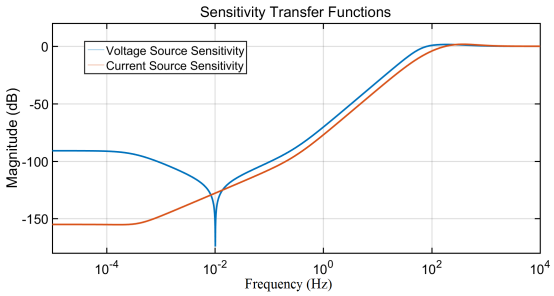

Fig. 7: Bode plot of sensitivity closed loop systems.

and current source regions, respectively. It is observed that the PV controller synthesized for current source region is more robust to variation in load requirements compared to its voltage source counterpart. Closed-loop sensitivity transfer functions (see Fig. 7) of current source and voltage source systems have bandwidths of 100 and 55 Hz, which are sufficiently large to handle variation in solar irradiance and temperature.

B. Voltage Set-Point Tracking With Sudden load Change

In the second case, V_{ref} is given as a sinusoid command from 100V to 500V with a frequency of 20rad/s. Fig. 6 (c) shows voltage source region controller tracking the sinusoid with voltage flattening at $\approx$ 180V. Reason for voltage flattening lies in the fact that for this PV setup $V_{\text{OC}} \approx 180$V and boost converter can only step up the input voltage; hence the output voltage cannot reach below $V_{\text{OC}} \approx 180$V. Fig. 6 (d) shows PV current source region controller tracking sinusoid reference with high accuracy and small voltage drop at 0.5 second, which corresponds to sudden change in load. As before, PV current source region controller shows better reference tracking capability and robustness.

VI. CONCLUSION AND FUTURE WORK

In this paper, we propose a new framework to address the problem of DC-link voltage regulation using a PV module. The algebraic structure of PV equations, and the time-scale separation between the fast PV dynamics and the slow variations in weather conditions are exploited to obtain simplified linearized models for a PV interfaced to the DC-link via a boost converter. The controllers exhibit excellent DC-link voltage tracking performance under varying loads and irradiance, and robustness to parametric uncertainties.

The setup to demonstrate the proposed control architecture is under preparation and the experimental results will be reported soon in our subsequent work.

APPENDIX

Proof of Claim 1

Proof: First, we identify an operating point for PV interfaced DC/DC converter in Fig. 4. Let V_{ref}, I_{SC}, and R denote the desired DC-link voltage, current output of the PV module at a given set of weather conditions and load resistance, respectively. The operating point I_L for the inductor current is obtained by setting the derivatives in (18) and (19) to zero at $v = V_{\text{ref}}$. This results in the following constraint equation,

$$(I_{\text{SC}} I_L - I_L^2)\frac{\alpha_i}{\alpha_v} - \frac{V_{\text{ref}}^2}{R} = 0. \tag{23}$$

Denote the perturbation in i_L about I_L by $\hat{i}_L$, i.e., $i_L = I_L + \hat{i}_L$. We aim to show that if the DC-link voltage is regulated at $v = V_{\text{ref}}$, then the inductor current i_L converges to I_L in the steady state.

Note that when $v \equiv V_{\text{ref}}$, then from (18) $u := d' i_L v \equiv V_{\text{ref}}^2/R$. Therefore (19) reduces to

$$\frac{1}{2}L\frac{d(I_L+\hat{i}_L)^2}{dt} = (I_{\text{SC}}(I_L+\hat{i}_L) - (I_L+\hat{i}_L)^2)\frac{\alpha_i}{\alpha_v} - \frac{V_{\text{ref}}^2}{R}. \tag{24}$$

After ignoring the second-order perturbations, (24) reduces to

$$I_L L\frac{d\hat{i}_L}{dt} \approx \underbrace{\left\{(I_{\text{SC}} I_L - I_L^2)\frac{\alpha_i}{\alpha_v} - \frac{V_{\text{ref}}^2}{R}\right\}}_{=0 \quad \text{from (23)}} + (I_{\text{SC}}\hat{i}_L - 2I_L\hat{i}_L)\frac{\alpha_i}{\alpha_v}, \tag{25}$$

which reduces to the following linearized form

$$\frac{d\hat{i}_L}{dt} = \frac{\frac{\alpha_i}{\alpha_v}(I_{\text{SC}} - 2I_L)}{LI_L}\hat{i}_L. \tag{26}$$

In constant current mode of operation, the inductor current at the operating point $I_L \approx I_{\text{SC}}$; since the equivalent resistor $\frac{\alpha_i}{\alpha_v}$ is very large and acts like an open-circuit. Therefore, $I_{\text{SC}} < 2I_L$. Hence (26) reduces to,

$$\frac{d\hat{i}_L}{dt} = -\alpha\hat{i}_L, \tag{27}$$

where $\alpha = \frac{\alpha_i}{\alpha_v}(2I_L - I_{\text{PV}})LI_L > 0$. Note that (27) represents asymptotically stable dynamics of the linearized system. Therefore, the inductor current i_L converges to value I_L locally. ■

REFERENCES

[1] M. Baranwal, S. M. Salapaka, and M. V. Salapaka, "Robust decentralized voltage control of dc-dc converters with applications to power sharing and ripple sharing," in *2016 American Control Conference (ACC)*. IEEE, 2016, pp. 7444–7449.

[2] J. J. Nedumgatt, K. Jayakrishnan, S. Umashankar, D. Vijayakumar, and D. Kothari, "Perturb and observe mppt algorithm for solar pv systems-modeling and simulation," in *2011 Annual IEEE India Conference*. IEEE, 2011, pp. 1–6.

[3] R. I. Putri, S. Wibowo, and M. Rifai, "Maximum power point tracking for photovoltaic using incremental conductance method," *Energy Procedia*, vol. 68, pp. 22–30, 2015.

[4] R. Rawat and S. Chandel, "Hill climbing techniques for tracking maximum power point in solar photovoltaic systems-a review," *Int. J. Sustain. Dev. Green Econ.(IJSDGE)*, vol. 2, pp. 90–95, 2013.

[5] E. Lorenzo, *Solar electricity: engineering of photovoltaic systems*. Earthscan/James & James, 1994.

[6] A. Kertesz, "Modeling and robust control design for distributed maximum power point tracking in photovoltaic systems," Ph.D. dissertation, University of Toronto, 2012.

[7] W. Xiao, W. G. Dunford, P. R. Palmer, and A. Capel, "Regulation of photovoltaic voltage," *IEEE Transactions on Industrial Electronics*, vol. 54, no. 3, pp. 1365–1374, 2007.

[8] R. W. Erickson and D. Maksimovic, *Fundamentals of power electronics*. Springer Science & Business Media, 2007.